mathematics

MDPI

Article

Estimation of the Spatial and Temporal Distribution of Magnetic Fields around Overhead Power Lines—A Case Study

Ionel Pavel, Camelia Petrescu *, Valeriu David and Eduard Lunca

Faculty of Electrical Engineering, "Gheorghe Asachi" Technical University of Iasi, 700050 Iasi, Romania; ionel.pavel@academic.tuiasi.ro (I.P.); valeriu.david@academic.tuiasi.ro (V.D.); costel-eduard.lunca@academic.tuiasi.ro (E.L.)

* Correspondence: camelia-mihaela.petrescu@academic.tuiasi.ro

Abstract: Due to the growing number, diversity and spreading of magnetic field sources, an increasing need to determine the field levels of human exposure has arisen. Some of the most encountered sources are the overhead power lines (OPL) and the determination of spatial and temporal variation of the magnetic fields produced by OPLs is a challenge. In this paper a hybrid method for the estimation of the temporal and spatial distribution of the magnetic flux density B caused by OPLs, based on experimental measurements and on numerical and analytical simulations, is presented. Thus, using a small number of simultaneous spot measurements correlated with a long-term survey, maps of the magnetic flux density distribution on extended areas are established, for several time instances. The proposed method is verified using two sets of different measurements and the results obtained through simulation. The difference between the estimated and simulated values of B is under 5.5%, which is considered acceptable considering that B spans over a large set of values (724 nT ÷ 1375 nT) in the location of the long-term survey procedure. The possibilities and limitations of the proposed method are discussed.

Keywords: magnetic field survey; experimental determination of magnetic fields; modeling and simulation of OPLs

MSC: 94C60

Citation: Pavel, I.; Petrescu, C.; David, V.; Lunca, E. Estimation of the Spatial and Temporal Distribution of Magnetic Fields around Overhead Power Lines—A Case Study. *Mathematics* **2023**, *11*, 2292. https://doi.org/10.3390/math11102292

Academic Editor: Jacques Lobry

Received: 23 April 2023
Revised: 10 May 2023
Accepted: 13 May 2023
Published: 15 May 2023

1. Introduction

Electrical energy transport and distribution is done through overhead power lines (OPLs) as well as, where necessary, through underwater sea cables buried in the sea bed. The development of industrial and household applications both in urban and in rural areas lead to an expansion of the distribution networks so as to satisfy consumer demands. This means a network of high voltage power lines, as well as medium and low voltage lines is geared towards the end consumer. Overhead power lines, which host currents in the order of hundreds of amps, produce magnetic fields whose levels must be monitored due to the possible adverse effects on people and other living beings.

Overhead power lines work in the extra low frequency domain of the electromagnetic spectrum (ELF), i.e., 30–300 Hz. The current view, resulting from numerous researches and measurements, is to achieve a prudent avoidance of the exposure to electric and magnetic fields, both in occasional and in occupational situations.

Even if the maximum admissible values recommended by several international regulating authorities are rather large (of the order of 100 μT for the magnetic flux density), in cases of exposure for long periods of time, the threshold for B must be significantly smaller, especially for children, hence the necessity of a long-term survey and that of a complete characterization of the magnetic field exposure for the general population [1–4].

Numerous researches addressed the problem of determining, both analytically and experimentally, the electric and magnetic field produced by OPLs, trying to include various aspects such as ground proximity or the proximity of other conductors, the deformation of line conductors due to gravity, etc. In the following, a brief overview of some recent papers that address this subject is given.

In [5], the formulae for computing the electric and magnetic field produced by a line current at high altitudes (110 km above the Earth's surface) are developed. The model considers a flat Earth surface and a multilayer soil structure, with different electric properties, and uses a series expansion technique and the complex image method, as well as exact integral expressions for $\bar{E}$ and $\bar{B}$ components based on Maxwell's equations and boundary conditions at the Earth's surface.

In [6], the authors use double complex numbers to incorporate in one expression the components of $\bar{B}$, B_x and B_y (and the fact that these are complex numbers). Closed form expressions are derived for $\bar{B}$, based on the Biot Savart Laplace (BSL) formula.

In [7], the relations for the computation of the electric and magnetic fields produced by finite length OPLs, using the classical expression for the magnetic vector potential, are established.

Paper [8] considers a 3D model of OPLs, with deformation of the lines due to gravity. The study combines the classical simulation current method (SCM) which replaces the actual unknown distribution of currents with simulated currents (in order to determine the magnetic fields) with two stochastic optimization methods, Particle Swarm (PS) and Differential Evolution (DE), used to optimize (determine) the position and number of simulated currents.

Another optimization method, Ant Lion Optimization (ALO), is used in [9] to determine the position of the overhead power line conductors that minimize both the electric and magnetic fields at a height of 1 m above the ground. This method of field reduction implies, however, additional costs, due to the necessity to re-design OPLs.

In [10], the authors propose a method for the analysis of multi-circuit overhead transmission lines using artificial neural networks (ANN) trained to estimate the real and imaginary parts of B_x and B_y at arbitrary points (x, y). The results are compared with BSL simulations and experimental measurements.

The magnetic field produced by submarine power cables is studied in papers such as [11], where closed form solutions for thin wires with a helical shape are established, as well as in [12], where both modelled and measured results for B are presented and the geomagnetic field is also taken into account.

The main objective of the present paper is to obtain a complete characterization of the magnetic field generated by overhead power lines in cases of long-term exposure, taking into account that B (rms) has large and unpredictable variations in time. The originality and novelty of the paper resides in the proposed hybrid method for estimating B using a correlation between spot measurements and long-term survey data. Both these measurements are made simultaneously using two measuring devices realized by the authors. Thus, maps with the spatial distribution of B in a large area near the OPL can be obtained for any moment of time, without the need of using a large network of sensors for measuring the magnetic flux density.

The results obtained using the proposed hybrid method and our instruments are in good agreement with the results obtained in simulations.

The organization of the paper is as follows: Section 2 presents the materials and methods used in the study, Section 3 presents the performed measurements, Section 4 presents the results of simulations, Section 5 discusses the obtained results and Section 6 is reserved for the conclusions of the paper.

2. Materials and Methods

Magnetic flux density can be expressed in a three-orthogonal system as:

$$B = \sqrt{B_1^2 + B_2^2 + B_3^2} \quad (1)$$

where B_1, B_2 and B_3 are the rms values of the components along the orthogonal directions. If the orthogonal system is Oxyz, then the three components are B_x, B_y and B_z. This simple observation ensures the fact that if the measurements are done with a sensor that determines the rms value of B, then the result is the same, irrespective of the sensor orientation.

The usual approach in monitoring the magnetic field produced by OPL is to trace a longitudinal and a transversal profile of B. If a mesh with a step size of 1 m is considered and measurements are conducted using only one instrument, the map for B is correct, if the current in the OPL is constant (rms) during the entire survey. Due to the fact that line currents are unpredictable, the magnetic field may vary significantly in the observation points, so a time variation for B (rms) must be also determined.

The method proposed in this paper takes into account both the spatial and the temporal variation of B (rms). The results are based on experimental determinations onsite and also on measurements and simulations (being thus a hybrid method). The experimental results are compared with the results obtained through numerical simulations that use the OPL configuration and the values of the line currents.

As a result of applying the proposed method, the spatial distribution (map) for B is obtained in a rectangular region with the dimensions (in this case study) of 60 m in transversal direction and 282 m in longitudinal direction, for any observation time during the automatic monitoring interval.

The geometric configuration of the OPL (2D transversal view) is outlined in Figure 1a and in Figure 1b. The real view of the line, with the measuring instruments, is presented.

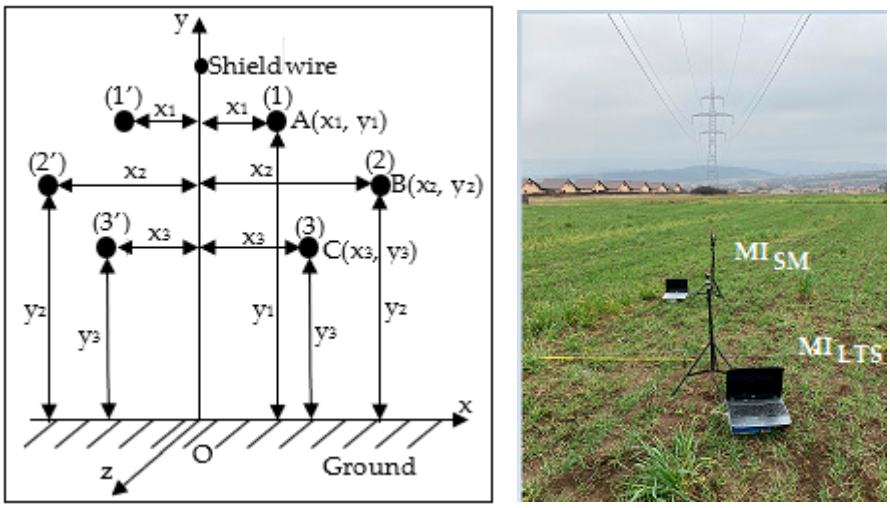

(**a**) (**b**)

Figure 1. (**a**) 2D cross section of the overhead power line, (**b**) real view of the OPL with the two measuring instruments (MI_{LTS} and MI_{SM}).

2.1. Measurement Procedure

The measurements for B are carried out using two instruments for automatic survey of the magnetic field, which were designed by the authors and are presented in Section 3.1 (Instrumentation). One of the instruments, MI_{LTS}, used for long-term survey, is placed in a fixed point under the geometric center of the OPL, at the mid-distance between two consecutive pillars. This instrument performs a survey for several hours, but this time can be increased to days or even months if proper housing and power supply is available.

The long-term survey performed by MI_{LTS} records the rms values of B for almost 6 h (5 h and 31 min) with a time step of about 1 s.

The second measurement instrument, MI_{SM} (Figure 1b), realizes spot measurements for B in the specified points of the longitudinal (LD) and transversal (TD) directions (with respect to the OPL), at points 1 m apart for TD and 3 m apart for LD. Unlike the procedure presented by the authors in [13], which used a simple commercial instrument for spot measurements, the procedure used in this paper is based on two automatic monitoring systems.

In this way, besides a very good synchronization between the two instruments (MI_{SM} and MI_{LTS}), i.e., the spot measurements data and the long-term survey data necessary for the proposed hybrid method, supplementary information regarding B are obtained in all the observation points.

The time for completing the spot measurements with MI_{SM} is approximately 20 min for the transversal profile and 40 min for the longitudinal profile, in the case studied experimentally in this paper. Two transversal profiles were traced, one at the pillar ($z = 0$) and one at the mid-distance between consecutive pillars ($z = d/2$), where d is the distance between the two pillars. The second transversal profile was traced in order to verify and compare the results obtained with the proposed method, as will be later detailed.

The number of spot measurements in longitudinal direction can be reduced to one half due to the symmetry of the magnetic field with respect to the transversal middle plane $z = d/2$. A total of 61 spot measurements were taken in transversal direction at times t_{T1}, t_{T2},..., t_{T61} and 95 measurements in longitudinal direction at times t_{L1}, t_{L2},..., t_{L95}.

2.2. Proposed Hybrid Method

Due to the fact that the current rms values have a permanent variation, in this paper, a method is proposed for the estimation of the magnetic field produced by the OPL both in transversal and in longitudinal directions for a specified time, e.g., t_{T1}, for the entire transversal profile ($EP_T(t_{T1})$) and similarly at t_{L1} for the entire longitudinal profile ($EP_L(t_{L1})$).

The estimated magnetic flux density, B_e, is determined using the measured values B_m and, also, taking into account the time variation of B (rms) recorded in one single fixed point ($z = d/2$) during the long-term survey, B_{LTS}.

The transversal profile is traced sequentially, resulting in a set of data for B_m in 61 evenly spaced locations, namely B_m measured at point P_1 at time t_{T1}, and so on, $B_m(P_1, t_{T1})$, $B_m(P_2, t_{T2})$,..., $B_m(P_{61}, t_{T61})$. In the transversal profile estimated at time t_{T1} ($EP_T(t_{T1})$), the estimated value coincides with the measured value only at the first point P_1:

$$B_e(P_1, t_{T1}) = B_m(P_1, t_{T1}) \tag{2}$$

The next values will be estimated based on the values measured with MI_{SM} in subsequent points $P_2, P_3, \ldots, P_{61}$, taking into account the time variation of B recorded with MI_{LTS} at the fixed point. Thus, at point P_2 the estimated value B_e is the following:

$$B_e(P_2, t_{T1}) = B_m(P_2, t_{T2}) * B_{LTS}(P, t_{T1})/B_{LTS}(P, t_{T2}) \tag{3}$$

Relation (3) is based on system linearity and can be obviously rewritten in the form:

$$\frac{B_e(P_2, t_{T1})}{B_m(P_2, t_{T2})} = \frac{B_{LTS}(P,\ t_{T1})}{B_{LTS}(P,\ t_{T2})} \tag{4}$$

A similar procedure is employed for estimating the longitudinal profile, $EP_L(t)$, at a given time t, using the data measured with MI_{SM} for B along the line and the values recorded by MI_{LTS} in a fixed observation point P.

According to this procedure, the estimated values should be the same as those measured simultaneously in all the 61 discretization points for the transversal profile and in all the 95 points for the longitudinal profile (if such an experiment were realized), but this would require a very large number of instruments (MI_{SM}), thus being impractical.

Using the consecutive measurements for one transversal profile (P_T) and one longitudinal profile (P_L), measured with MI_{SM}, and the values for B obtained during the long-term survey in a fixed point (measured with MI_{LTS}), the transversal profiles for any $z = k \cdot d/N, k = \overline{0, N}$, where d/N is the step size in longitudinal direction, can be estimated for any moment of time. At the same time, the longitudinal profiles for any time during the observation procedure with MI_{LTS} can be also estimated.

Using this method, a matrix of 61×95 points (for the considered step size), containing the estimated values of B in a rectangular region under the OPL covering an area of 60 m $\times$ 282 m, is obtained for any moment of time during the survey with MI_{LTS}. Maps with the estimated values of B can be generated in MATLAB using these matrices.

2.3. OPL Modeling

The transversal view of the overhead power line is presented in Figure 1. In order to determine the magnetic flux density, both an analytical and a numerical approach can be used. In this paper the focus is on the magnetic field (the electric field is not monitored), so that the ground proximity of the line conductors plays a less important role since the Earth's magnetic permeability is close to μ_0. Moreover, as stated before, the OPL works at 50 Hz (extra low frequency domain) which further simplifies the analysis. At such a low frequency, the wavelength is of the order of thousands of km, and the propagation of the electromagnetic field, which occurs in direction Oz (along the line) is characterized by the Poynting vector S.

$$\bar{S} = \bar{E} \times \bar{H} = \left(E_x \bar{i} + E_y \bar{j}\right) \times \left(H_x \bar{i} + H_y \bar{j}\right) = \left(E_x H_y - E_y H_x\right) \bar{k} \tag{5}$$

where $\bar{i}$, $\bar{j}$ and $\bar{k}$ are the unit vectors of the three axes Ox, Oy and Oz. In sinusoidal steady state, the vectors are complex. Comparing the dimensions of the line, which may be of the order of tens of kilometers, to the wavelength, we can assert that the line is in quasi-stationary magnetic regime. This means that the time variation of the electric field is negligible, and the equations for the determination of the magnetic field are the same as in stationary regime:

$$\nabla \times \bar{H} = \bar{J}\ ; \bar{B} = \mu \bar{H}\ ; \nabla \cdot \bar{B} = 0 \tag{6}$$

Thus, in an environment of constant permeability μ_0, the magnetic flux density produced by a thin conductor can be determined using the Biot–Savart–Laplace formula (BSL):

$$\bar{B}(P) = \frac{\mu_0 i}{4\pi} \oint_{\Gamma} \frac{\bar{dl} \times \bar{R}}{R^3} \tag{7}$$

which, for the long line conductor, becomes (Figure 2b) the following:

$$\underline{\bar{B}}_k = \frac{\mu_0 \underline{I}_k \left[(y - y_k) \bar{i} + (x_k - x) \bar{j} \right]}{2\pi \left[(x - x_k)^2 + (y - y_k)^2 \right]} \tag{8}$$

In (8), $\underline{I}_k$ is the complex rms value of the current in conductor k. In the case of the OPL line, there are six conductors which may or may not be current-carrying conductors (some currents may be zero).

The total magnetic field is obtained by superposition:

$$\underline{\bar{B}} = \sum_{k=1}^{6} \underline{\bar{B}}_k \tag{9}$$

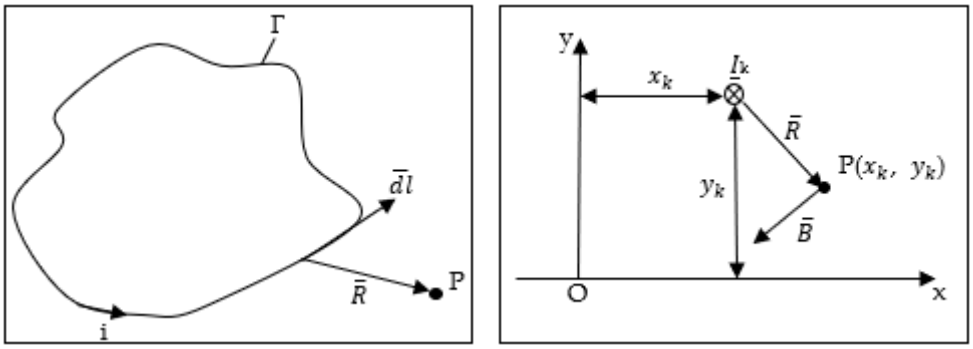

(**a**) (**b**)

Figure 2. Determination of the magnetic flux density with the BSL formula: (**a**) general case, (**b**) line conductors.

3. Measurements

3.1. Instrumentation

The proposed hybrid method is based on the data obtained during the automatic long-term survey performed using the two instruments MI_{SM} and MI_{LTS}. These new/original instruments were designed, realized and calibrated by the authors [14–16] for the purpose of measuring magnetic fields, being suitable in monitoring magnetic field exposure for the general population.

Although there are small differences between MI_{SM} and MI_{LTS}, each of the two instruments consists of an isotropic field sensor (three linear coils), an electronic signal processing circuit (amplifier and integrator), a data acquisition module and a laptop that hosts several virtual instruments realized in LabVIEW.

Both measurement systems record and process the waveforms for the three components of B. The processing and LabVIEW module can perform a frequency analysis and compute the rms and peak-to-peak values, as well as a statistical post-processing of the recorded data. These two instruments can perform a long-term survey of the magnetic field, recording samples of B every second for a frequency range of the B components up to 100 kHz, which is appropriate for observing the biological effects of the magnetic field.

The calibration of these instruments was conducted using a reference magnetic field (standard-field method), with an uncertainty of less than 5%. This uncertainty of the measurement instrument was also verified by comparison with commercial instruments.

The experimental recording performed with MI_{LTS} lasted for 5 h and 31 min, between 9:37 am and 3:08 p.m. At the same time interval, the transversal profiles near the pillar (in z = 0) and at the mid-distance between two pillars (z = d/2), and also the longitudinal profile B (0, y, z), z ∈ [0, d], were traced with MI_{SM} at a height y = 1 m above the ground.

The OPL considered in experiments (Figure 1b) is a double three-phase line 2 × 220 kV with RST-RST phase disposition, situated in Iasi County, Romania. The geometrical configuration of the line as well as the current rms values are known and are used in the numerical simulations.

3.2. Measurement Results

During the experiments, two profiles for B were obtained: one in transversal direction for z = 0, P_T, and a longitudinal profile P_L for z ∈ [0, d]. A supplementary verification and validation of these results is performed using measurements taken for a transversal profile at the mid-distance between two consecutive pillars, P_{TM}.

Figure 3 depicts the transversal profile near the pillar using 61 consecutive measurements in points 1 m apart, at different moments of time (since only one instrument MI_{SM} was used). The maximum value for |B| is obtained at approximately 5 m from the central symmetry plane of the OPL, due to the fact that the currents in the second line (conductors (1′), (2′) and (3′) in Figure 1) were zero (line out of service).

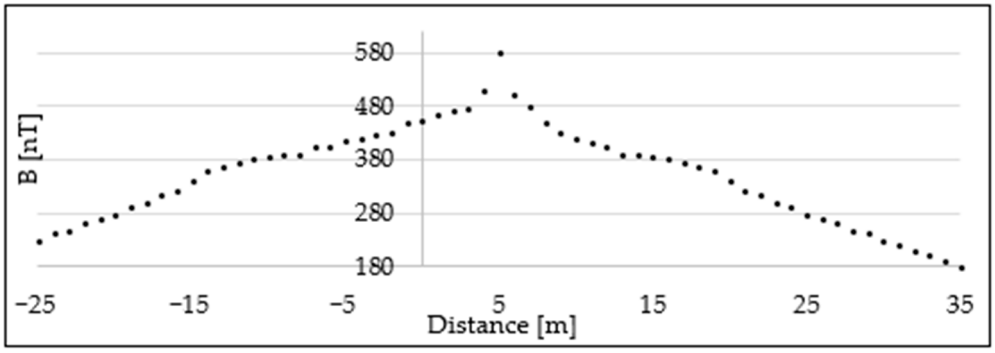

Figure 3. Transversal profile for |B| obtained in successive measurements near one pillar (z = 0).

The longitudinal profile between two pillars, P_L, was traced using spot measurements in points 3 m apart for the distance d = 282 m, Figure 4. In the considered case, the experimental procedure for P_L lasted 40 min.

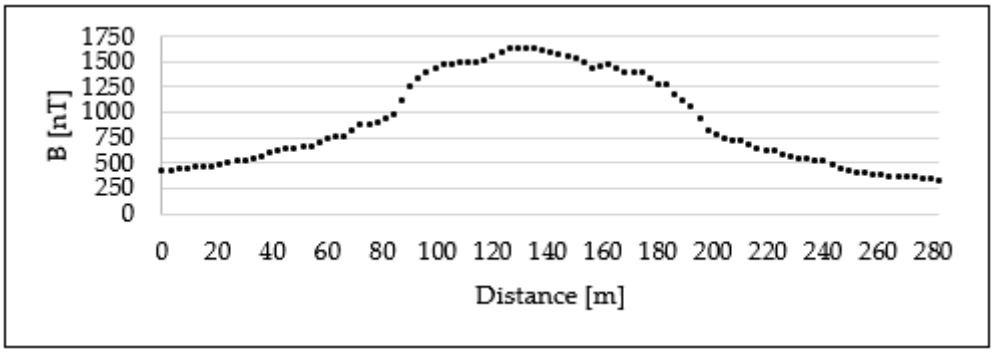

Figure 4. Longitudinal profile for |B| obtained in successive measurements (P_L).

The plots in Figures 3 and 4 show rather large variations of |B|, even for neighboring points. This is due to the variation of $|I_k|$ in time, allowing for the instrument MI_{SM} to be moved to the next position.

However, most of these variations can be smoothed (leveled) using the proposed method for estimating the magnetic field profile at a given time, this being equivalent to the case when all the measurements are carried out simultaneously. Some irregularities in |B| still persist even after applying this method due to errors produced by the fact that the Earth's surface is not flat (small differences in the distance between the line and the instrument occur).

Although the profiles P_T and P_L give sufficient data in order to plot a map of |B| in a rectangular region beneath the line, a second transversal profile P_{TM} was recorded at a distance z = d/2. This profile, represented in Figure 5, is used to verify the proposed method for field estimation. The procedure is based on the comparison of the data in P_{TM} with the transversal profile estimated using the data in P_T, taken in z = 0, the data in P_L and the time variation of B obtained with MI_{LTS} during the long-term survey.

Thus far, only the data from spot measurements with MI_{SM} were presented. In the following, the data from the long-term survey performed with MI_{LTS} will be presented and discussed. Figure 6 presents the recordings made for B rms with MI_{LTS} for the entire observation interval of 5 h and 31 min. In this recording, a significant temporal variation of the magnetic field can be observed, justified by the time variation of the rms current in the line. These variations can be correlated with the variations of B identified in the measured data for the longitudinal profile (plotted in Figure 4).

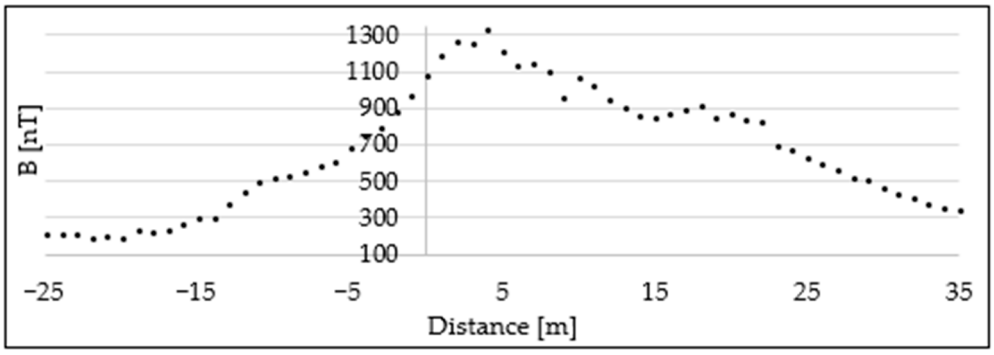

Figure 5. Transversal profile measured experimentally at the mid-distance between two pillars.

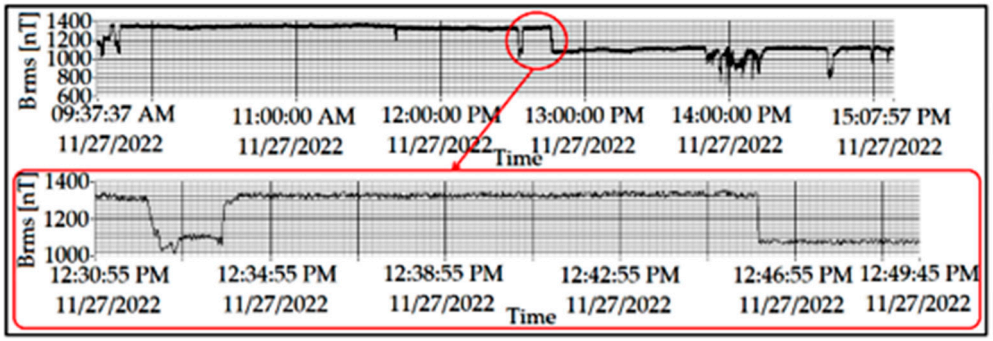

Figure 6. Values recorded for B (rms) during the long-term survey at a fixed point.

Using the long-term survey instrument, MI_{LTS}, a time and frequency analysis of the recorded signal can be performed. Figure 7 presents both the time variation and the spectral analysis for the field components B_x, B_y and B_z.

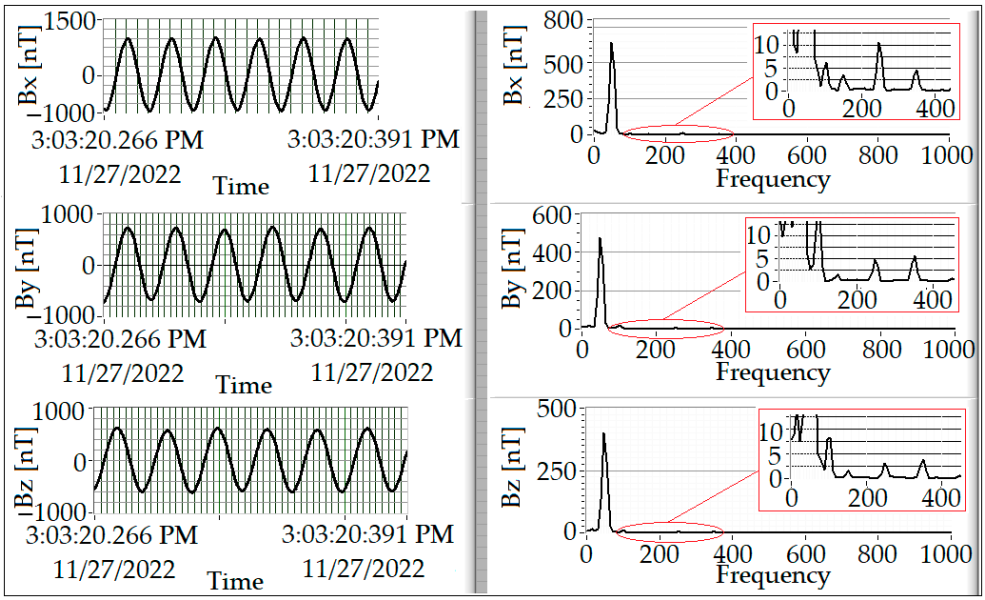

Figure 7. Waveforms and spectral analysis for the B components.

A statistical post-processing of the recorded results over the observation time interval can be also performed. Table 1 presents the results of post-processing, i.e., date and time of observation, number of measurements, minimum, maximum and average values of B, standard deviation, number of recorded data larger than the average value and percentage of exceeding values.

Table 1. Post-processing statistical results for the data recorded with MI_{LTS}.

Survey Period [hh:mm]	Number of Measurements	Min.	B_{rms} [nT] Average	Max.	Standard Dev.	$\frac{t_{over\ average}}{t_{survey}} \times 100(\%)$
[05:31]	17,530	724	1223	1375	132.3	54.67

The currents in the line, further used in simulations, are known only for six moments in time (10 a.m., 11 a.m.,..., 3 p.m.), but the number of values recorded for B during the long time survey is 17,530, with a time step of about 1 s (17,530 measurements in 19,860 s). Moreover, if the range for the current rms values is from 118 to 196 A, the range of values for B recorded by MI_{LTS} is from 724 to 1375 nT.

4. Modeling and Simulation Results

4.1. Estimation Based on "In Situ" Field Measurements

Due to the time variation of the magnetic field rms value, tracing the transversal and longitudinal values is difficult to achieve using only one instrument. The objective of this paper is to obtain an estimation of the magnetic field at each point of a rectangular mesh beneath the OPL at a particular moment of time. This estimation is realized using the values of B obtained with the two instruments MI_{LTS} and MI_{SM} and then applying a correction to the values obtained at successive moments in time. In this way, all the values for B in each profile are estimated at the same moment of time as if simultaneous measurements were made in 61 points for the transversal profile and 95 points for the longitudinal profile.

Figure 8 presents three estimations of B for the transversal profile near the pillar at moments t_{Ti}, t_{Tj} and t_{Tk} (11 a.m., 12 a.m. and 1 p.m.), determined from the successive measurements recorded in P_T, performed with MI_{SM} and estimated according to relation (3). In Figure 8, the data from P_T (represented in Figure 3) are also included in order to observe the possibilities of the proposed method.

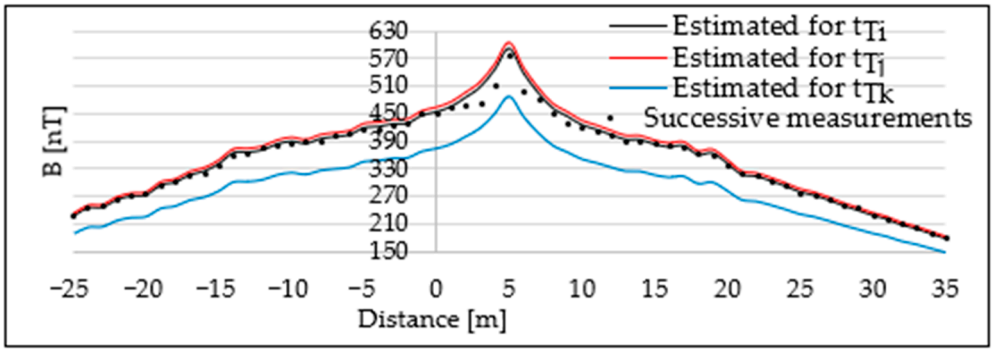

Figure 8. Transversal profiles near the pillar estimated at times t_{Ti}, t_{Tj} and t_{Tk}, compared to the results from spot measurements.

Using the same method, estimations for the longitudinal profile were also made at the moments t_{Li}, t_{Lj} and t_{Lk} (11 a.m., 12 a.m. and 1 p.m.). The estimated longitudinal profiles, as well as the original profile, are presented in Figure 9. As may be seen, the original large variations of B from Figure 4 are corrected, and the estimation results present a rather smooth variation.

In order to verify the proposed estimation method, similar estimations were made for the transversal profile P_{TM} (corresponding to z = d/2) for the chosen moments t_{TMi}, t_{TMj} and t_{TMk} (11 a.m., 12 a.m. and 1 p.m.). The resulting plots, as well as the original profile P_{TM}, are presented in Figure 10.

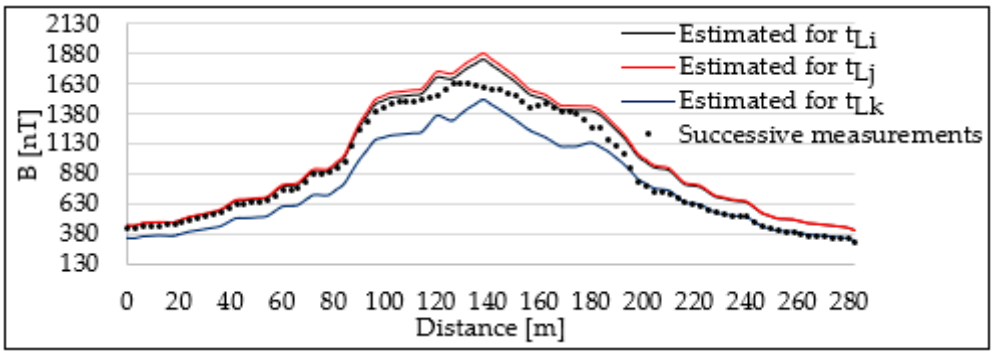

Figure 9. Estimated longitudinal profiles at times t_{Li}, t_{Lj} and t_{Lk} compared to the results from spot measurements.

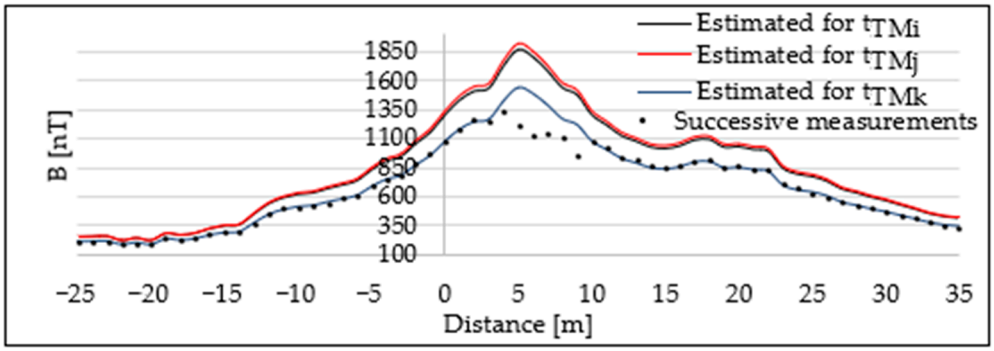

Figure 10. Transversal profiles at the mid-distance between the pillars, estimated at the moments t_{TMi}, t_{TMj} and t_{TMk}, compared with the experimental profile.

As mentioned before, the transversal profile P_{TM} was traced for $z = d/2$, but similar transversal profiles can be determined experimentally and then estimated according to (3) for any value $z \in [0, d]$.

Figure 11 presents two plots that estimate the transversal profile for B in $z = d/2$ at the same moment t_k (in the considered case at 1 p.m.), using two separate sets of experimental data, namely:

1. Data for the transversal profile at the pillar ($z = 0$) and for the longitudinal profile (obtained with MI_{SM}), taking also into account the temporal variation of B obtained in the long-term survey, thus resulting, firstly, in the estimated profiles $EP_T(t_k)$ and $EP_L(t_k)$ and finally the estimated transversal profile at the distance $z = d/2$ at time t_k;
2. Data from the experimental transversal profile P_{TM} at $z = d/2$, considering also the time variation recorded with MI_{LTS} at $z = d/2$, thus resulting in the estimated transversal profile at time t_k (as it was presented in Figure 10).

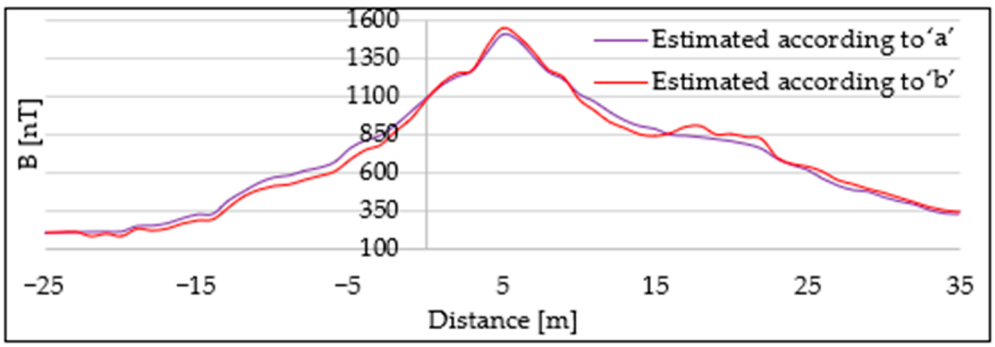

Figure 11. Estimated transversal profile at the mid-distance between two towers, based on two different sets of data correlated with the continuous recording of B_{LTS}.

Comparing the two plots in Figure 11, a relative deviation of under 9% is observed in the conditions in which the range of the recorded values for B is from 724 to 1375 nT, and other factors, such as instrument error (under 5%), terrain oscillations, small errors in positioning the instrument MI_{SM}, etc., affect the measured values of B.

In a similar manner, the transversal profiles for any value of z can be obtained using one transversal profile (P_T) measured at a fixed point z_0, the longitudinal profile P_L and the time recordings for B conducted with MI_{LTS}.

Using this method for estimating the magnetic field in transversal direction for any $z \in [0, d]$, maps of the magnetic field in a rectangular region beneath the OPL can be obtained for any of the 17,530 moments of time for which recordings of B performed with MI_{LTS} exist (Table 1).

Figures 12 and 13 represent a map of $|B|$ in the region $z \in [0, d]$, $x \in [-x_{max}, x_{max}]$, with d = 282 m, $x_{max} = 30$ m, in two cases: for a time t_X when the estimated value of B is equal to the maximum value obtained in the long-time survey, and for a time t_y when the estimated value of B is equal to the minimum recorded value of B. These maps can be obtained using only one longitudinal and one transversal profile, resulting in a significant reduction of the number of spot measurements.

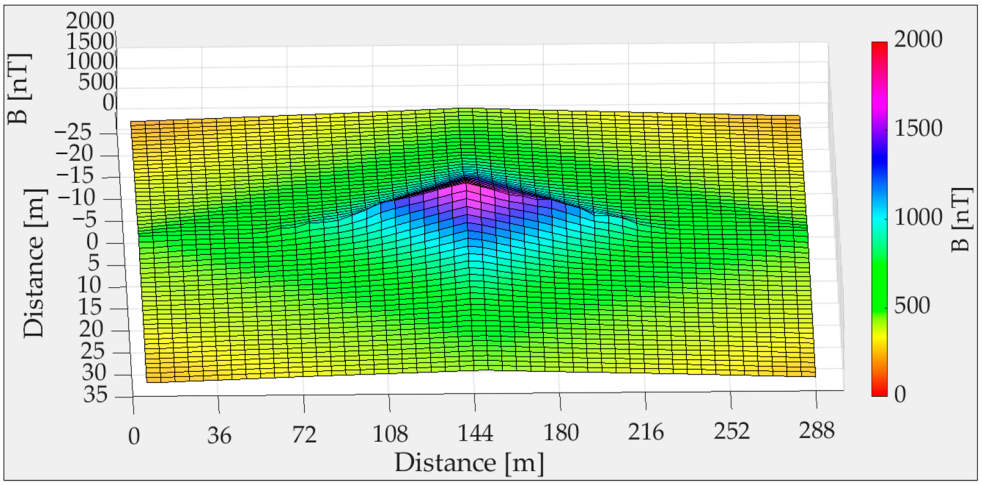

Figure 12. Magnetic flux density map for the maximum recorded value of B.

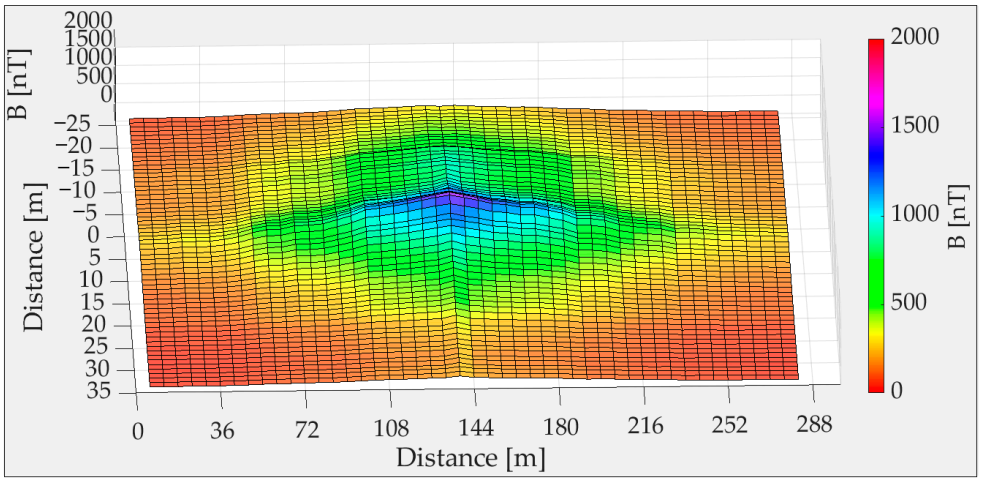

Figure 13. Magnetic flux density map for the minimum recorded value of B.

4.2. Results of Analytical and Numerical Simulations

The transversal profile for the norm of the magnetic flux density

$$\left|\underline{\bar{B}}\right| = \sqrt{\left|\underline{B}_x\right|^2 + \left|\underline{B}_y\right|^2} \tag{10}$$

calculated with relations (8)–(10), is presented in Figure 14 for the cases in which the experimental data obtained with MI_{LTS} were available and the values of the rms line currents are known. Conductors (1)–(3) (Figure 1a) carry a symmetric three-phase current, with values specified in Figure 14 (three cases), while the current in the conductors (1′), (2′) and (3′) are zero (line not in service). The geometric coordinates considered in simulations, corresponding to the position of the three conductors at the pillar, are $x_1 = 5$ m, $y_1 = 35$ m, $x_2 = 8$ m, $y_2 = 28.5$ m, $x_3 = 5$ m and $y_3 = 22$ m.

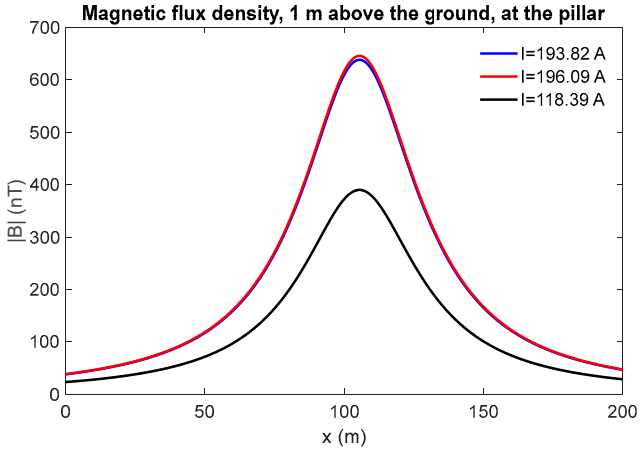

Figure 14. Transversal profile of |B| at the pillar—simulations based on analytical results.

A numerical simulation of the line was also performed using COMSOL Multiphysics 6.1. In this case, the electrical constants for the soil, ε_r and σ can be also taken into account, but these constants depend on the content of water in the soil [17]. In the numerical simulations, the considered values were $\sigma_{soil} = 0.5$ S/m and $\varepsilon_{r\,soil} = 10$.

The transversal profile for the magnetic flux density at the height of 1 m and 1.8 m, respectively, above the ground, was computed using the same geometric coordinates for the conductors as before (conductors near the pillar), and the results are presented in Figure 15. Simulations for other numerical values of σ_{soil} and $\varepsilon_{r\,soil}$ were also carried out since their value in the onsite experiment is uncertain, but it was found that they have a small influence over B.

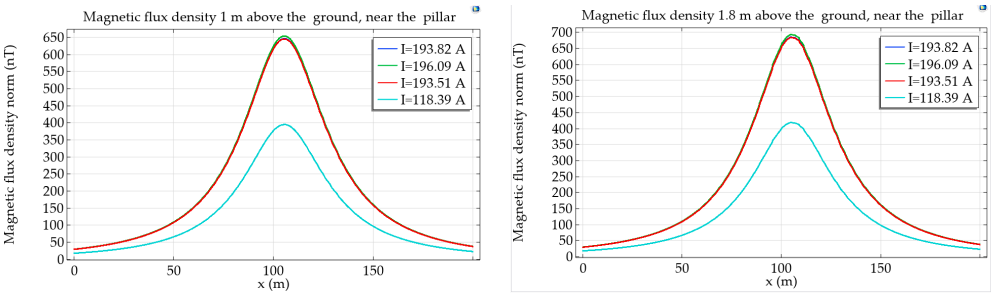

(**a**) (**b**)

Figure 15. Transversal profile of |B| at the pillar—simulations in COMSOL: (**a**) at a height of 1 m above the ground, (**b**) at a height of 1.8 m above the ground.

In Figures 14 and 15 the geometric plane of symmetry of the OPL is the plane x = 100 m. In the COMSOL simulations, the physics module magnetic and electric fields (mef) was used, performing a frequency analysis [18]. The plots in Figure 15 correspond to 50 Hz. This physics module takes into account the displacement currents, besides the conduction currents, making the study more accurate. The dimensions of the entire analyzed domain were 400 m in the direction of Ox and 300 m in the direction of Oy, with a 150 m region under the ground.

The results obtained in the COMSOL simulations are in very good agreement with the analytical results. For example, the largest value of B, obtained for I = 193.82 A, is B_{max} = 646 nT in COMSOL and 638 nT in MATLAB (analytical results), giving a maximum relative difference between analytical and numerical simulations of 1.2%.

Comparing the results obtained in simulations with the estimated values of B obtained using the hybrid method (Section 4.1), the similarity of the plots in Figures 8 and 14 (or Figure 15) can be observed with inherent irregularities in the curve based on the experiment, due to the particular onsite conditions (as mentioned in 4.1). At the same time, the maximum value of B is 638 nT in the analytical simulations (for I = 193.82 A) and from the estimations based on the measurements B_{max} = 605 nT, leading to a maximum relative difference between the simulated and estimated B of 5.4%.

5. Discussions

In order to obtain a complete map of the magnetic flux density produced by an overhead power line (OPL), a large number of simultaneous measurements taken over a significant time interval would be necessary. This approach that takes into account the spatial and temporal variation of B (rms) is not feasible due to the large number of instruments necessary in the survey and the complexity of the entire operation.

That is why characterization of the magnetic fields produced by the OPL is usually performed using a transversal and a longitudinal profile obtained in successive measurements in a number of observation points. This approach is easier to implement and needs only one measurement instrument, but it is not complete because it does not distinguish between the spatial and temporal variations of B and becomes incorrect when the magnetic field has large variations in time, which happens in most cases.

The transversal profile P_T obtained through successive measurements and presented in Figure 3 is able to characterize the magnetic field in the direction perpendicular to the line, since B has small variations at the time these data were collected. The small deviations from the real values can be caused by terrain oscillations of levels and small errors in positioning the instrument.

In contrast, the longitudinal profile P_L, obtained experimentally through successive measurements and presented in Figure 4, cannot characterize correctly the spatial variation of B along the line in direction Oz, due to the large variations of B during the experiment.

That is why, in this paper, a new method for estimating the longitudinal profile and the transversal profiles for B at different positions along the line ($z \in [0,d]$) is proposed, thus allowing for spatial maps of B to be represented at different moments of time. In the case considered in this study, the map for B covers an area of 60 m $\times$ 282 m. In order to obtain the estimated profiles for B, two instruments are used, one for spot measurements in different points (MI_{SM}) and one for a long-term survey (MI_{LTS}), which record automatically and continuously the values of B in a fixed point. Thus, using only two instruments, 156 values for B are collected using MI_{SM} (61 for P_T and 95 for P_L) and, using MI_{LTS}, the values of B can be estimated in 5795 points at any moment of time (17,530 instances of time, according to Table 1). Some of the estimated results are presented in Figures 8–11. Two maps for the magnetic flux density are also presented in Figures 12 and 13, at moments corresponding to the maximum and minimum recorded values of B, respectively.

The first validation of the proposed method is conducted within the method by obtaining two estimated transversal profiles at the mid-distance between two consecutive pillars P_{TM} (Figure 5). The plots in Figure 11 show that the two estimations for the same

profile at the same moment of time, obtained using two separate sets of data, are almost identical, with relative differences between the two profiles of under 9%.

In order to verify or validate the proposed method, calculations for B using analytical and numerical methods were also used. The maximum relative difference between the hybrid method and data from analytical simulations, using estimations of the transversal profile at the pillar, was 5.4%.

The two instruments MI_{SM} and MI_{LTS} were designed, realized and calibrated by the authors, with an uncertainty in the measured value of B of under 5%. Supplementary measurement uncertainty may also occur due to errors in positioning the instrument both in horizontal and in vertical directions and also due to possible errors in the time synchronization of the two instruments.

The proposed hybrid method of estimation may be used to map other sources of electromagnetic field, and, by using an automatic recording of the magnetic flux density and of the electric field, maps for both B and E can be obtained [14,15].

6. Conclusions

This paper presents a new hybrid method to estimate and map the magnetic flux density produced by overhead power lines in a large region beneath the OPL and for a long period of time using a minimized number of spot measurements and a long-term survey of B. The method is based on the correlation of data from a transversal profile and those from a longitudinal profile of B, obtained by successive measurements made in a short time interval, with the data from the long-term survey, both sets of data being obtained with instruments developed by the authors.

In order to validate the results of the estimations, simulations are carried out based on the analytical and numerical methods for magnetic field determination. The relative difference between the estimation and simulation results is under 5.5%.

All the measured, estimated and calculated values in the analyzed case are below the threshold imposed by international regulations for human exposure to magnetic fields. It is to be mentioned, however, that there are reports suggesting that long time exposure of children to magnetic fields in the ELF domain must be limited to much lower values than those recommended by international regulating organizations, this being a subject of ongoing research.

Thus, the need for estimating and mapping the magnetic field produced by OPL (an important source of magnetic fields) and characterizing the human field exposure to complex fields is a topic of major interest that relates to public health concerns.

Author Contributions: Conceptualization, V.D.; methodology, V.D., C.P. and I.P.; software, C.P.; validation, I.P., C.P. and V.D.; formal analysis, I.P. and C.P.; investigation, I.P.; resources, I.P. and E.L.; writing—original draft preparation, V.D. and C.P.; writing—review and editing, C.P.; visualization, C.P. and I.P.; supervision, V.D. All authors have read and agreed to the published version of the manuscript.

Funding: This research received no external funding.

Data Availability Statement: Not applicable.

Acknowledgments: This work was achieved through the Advanced Research postdoctoral program within IOSUD-TUIASI: "Performance and Excellence in postdoctoral Research—2022". The first author would like to thank for the support obtained through the project "Network of excellence in applied research and innovation for doctoral and postdoctoral programs"/InoHubDoc, a project co-funded by the European Social Fund.

Conflicts of Interest: The authors declare no conflict of interest.

Nomenclature

OPL	Overhead Power Line
B	magnetic flux density
rms value	root mean square value
MI_{LTS}	Measurement Instrument for Long-Term Survey
MI_{SM}	Measurement Instrument for Spot Measurements
P_L	Longitudinal profile (obtained from successive measurements)
P_T	Transversal profile (obtained from successive measurements)
P_{TM}	Transversal profile at the mid-distance between two consecutive pillars
t_{T1}, t_{T2},....., t_{T61}	times at which measurements were made in 61 points for the transversal profile
t_{L1}, t_{L2},....., t_{L95}	times at which measurements were made in 95 points for the longitudinal profile
EP_T (t_{T1})	estimated (whole or completed) transversal profile for time t_{T1}
EP_L (t_{L1})	estimated (whole or completed) longitudinal profile for time t_{L1}
d	distance between consecutive pillars of the OPL
B_e	estimated magnetic flux density
B_m	measured magnetic flux density in successive measurements with MI_{SM}
B_{LTS}	values of B measured with MI_{LTS} during the long-term survey

References

1. Directive 2013/35/EU of the European Parliament and of the Council. *Off. J. Eur. Union* **2013**, *179*, 12–18.
2. Tourab, W.; Babouri, A. Measurement and modeling of personal exposure to the electric and magnetic fields in the vicinity of high voltage power lines. *Saf. Health Work.* **2016**, *7*, 102–110. [CrossRef] [PubMed]
3. Garrido, C.; Otero, A.; Cidras, J. Low frequency magnetic fields from electrical appliances and power lines. *IEEE Trans. Power Deliv.* **2003**, *18*, 1310–1319. [CrossRef]
4. Bravo-Rodriguez, J.C.; del-Pino-Lopez, J.C.; Cruz-Romero, P. A survey on optimization techniques applied to magnetic field mitigation in power systems. *Energies* **2019**, *12*, 1332. [CrossRef]
5. Pirjola, R.; Boteler, D. Calculation methods of the electric and magnetic fields at the Earth's surface produced by a line current. *Radio Sci.* **2002**, *37*, 1–9. [CrossRef]
6. Filippopoulos, G.; Tsanakas, D. Analytical calculation of the magnetic field produced by electric power lines. *IEEE Trans. Power Deliv.* **2005**, *20*, 1474–1482. [CrossRef]
7. Vujevic, S.; Sarajcev, P.; Botica, A. Computation of overhead power line electromagnetic field. In Proceedings of the 16th International Conference on Software, Telecommunications and Computer Networks, Split-Dubrovnik, Croatia, 25–27 September 2008.
8. OuYang, W.; Zhang, J.; Hu, J.; Lv, W.; Wang, D. PSO/DE combined with simulation current method for the magnetic field under transmission lines in 3D calculation model. *Meas. Control.* **2022**, *55*, 1097–1109. [CrossRef]
9. Al Salameh, M.; Alnemrawi, S. Ant Lion optimization to minimize emissions of power transmission lines. *Progress Electromagn. Res.* **2022**, *110*, 171–184. [CrossRef]
10. Mujezinovic, A.; Turajlic, E.; Alihodzic, A.; Dautbasic, N.; Dedovic, M.M. Novel method for magnetic flux density estimation in the vicinity of multi-circuit overhead transmission lines. *IEEE Access* **2022**, *10*, 18169–18181. [CrossRef]
11. Scott, G.; Pooley, M.; Cotts, B. Numerical and analytical modeling of electromagnetic fields from offshore power distribution cables. *IEEE Trans. Magn.* **2023**, *59*, 1–5. [CrossRef]
12. Kavet, R.; Wyman, M.; Klimley, P. Modeling magnetic fields from a DC power cable buried beneath San Francisco bay, based on empirical measurements. *PLoS ONE* **2016**, *11*, e0148543. [CrossRef] [PubMed]
13. David, V.; Pavel, I.; Lunca, E. A method for estimating the magnetic fields generated by the overhead power lines. In Proceedings of the 11th International Conference and Exposition on Electrical and Power Engineering (EPE), Iași, Romania, 22–23 October 2020.
14. David, V.; Nica, I. A measurement system for an automatic survey of low frequency magnetic and electric fields. *Rev. Sci. Instrum.* **2012**, *83*, 105102. [CrossRef] [PubMed]
15. David, V.; Nica, I. System for Determination of Low Frequency Magnetic and Electric Fields. Patent 127139/30.09, 30 September 2014.
16. David, V.; Lunca, E.; Pavel, I. Automatic Monitoring for the Magnetic Fields with the Detection and Characterization of Transient Fields. Patent RO-BOPI 8/2019, 30 August 2019. pp. 36–37.
17. Scott, J. *Electric and Magnetic Properties of Rock and Soil*; Open-File Report 83-915; United States Department of the Interior Geological Survey: Reston, VA, USA, 1983. [CrossRef]
18. COMSOL Multiphysics v. 6.1 Documentation, AC/DC Module User's Guide. Available online: www.comsol.com (accessed on 1 February 2023).